academicJournals

Vol. 11(19), pp. 202-212, 15 October, 2016
DOI: 10.5897/SRE2016.6401
Article Number: 142DAB761024
ISSN 1992-2248

http://www.academicjournals.org/SRE

Scientific Research and Essays

Full Length Research Paper

Dynamic modelling and predictive health monitoring for vibration control and resonance of rotating machinery

A. Chellil[1]*, I. Gahlouz[2,3], S. Lecheb[1], S. Chellil[1], A. Nour[1] and H. Mechakra[1]

[1]Dynamic of Engines and Vibroacoustic Laboratory, Industrial Maintenance Department, Université M'hamed Bougara de Boumerdes, Algeria.
[2]Industrial Maintenance Department, Université M'hamed Bougara de Boumerdes, Algeria.
[3]Poly Tech. Lille, LAGIS CNRS UMR 8219, 59655, Villeneuve d'Ascq Cedex, France.

Received 27 March, 2016 Accepted 27 September, 2016

The aim of this study is to investigate the critical speed analysis and response of a rotating machinery. The search for increasingly high performances in the field of the vibration phenomena which is subject rotor are increasingly important and can lead to system instability. The use of the finite element method makes to establish dynamic equations of the movement. Numerical calculations of the model developed, can extract the natural frequencies and modal deformed of the rotor, and this reduce is nonlinear. The Campbell diagram plot used to determine the critical speeds. Experimentally the study of the rotor in transient system allowed the determination of the spectral responses due to the unbalances and various excitations.

Key words: Stability, rotor, dynamic, critical speed.

INTRODUCTION

A detailed understanding of vibration problems associated with rotating systems is currently a major issue in the industrial field. To optimize the dynamic behavior of rotors and dimension to the best of such systems, Stodola (1972) worked out an iterative method to calculate the fundamental frequency of a vibrating system based on a standard form of eigen mode; it has been noted that the gyroscopic effect is a factor impacting the critical speed of a rotor. Si-Chaib et al. (2008) presented models based on the finite elements of flexible rotors to calculate the critical speeds and the eigen modes. In these models, the gyroscopic effects and the axial loadings are not taken into account. In the last few years, the most employed model has been developed based on the finite element method (Nelson, 1980; Tran, 1981); which allowed the determination with good precision the eigen frequencies and the damping ratios, as well as the response to the various excitations. Moreover, this approach is modular because each element of the rotor is defined separately. Elements can thus be added or withdrawn according to the studied phenomena. The finite element method was thus used to study the embarked phenomena of damping in dynamics of the rotors (Duchemin, 2003). It was also applied to the study of the rotors whose shaft turns at variable speed (Al Majid, 2003). Many results concerning the dynamics of the rotors, whose support is fixed, have been reported for the models of Rayleigh-Ritz and the finite elements

*Corresponding author. E-mail: cchellil@yahoo.fr.

(Lalanne, 1998).

The experimental studies concerning the dynamics of the rotors are concentrated on inaccessible points by the theoretical way; these are the characteristics of bearing, dampings, actual stiffnesses, coefficients of sealing of the labyrinths and finally the flexibility of the foundations. Vance et al. (1987) compared the numerical and experimental results of the "free-free" modes and evaluate the precision of the model according to the coupling of the rotor with the discs. The Rayleigh-Ritz method is used to set up a model making it possible to treat simple cases and to highlight basic phenomena. A finite element model is developed to treat real systems. The equations of motion of the rotor are obtained by application of Lagrange equations.

The vibration indicators are used for fault detection and can track its evolution to manage the predictive maintenance

A fault diagnosis approach has been proposed by Wei et al., (2015) for rotating machines based on a new method for extracting and evaluating the statistical function; health condition is classified as the threshold corresponding is exceeded.

In this work, the dynamic behaviour of a rotor is discussed. The numerical study determines the deformed modes, evaluate Campbell's diagram and the response to the unbalance of the rotor in the vicinity of critical speeds.

The result for the estimation of the term vibration source on a particular line is shown in this paper, and the terms source estimated by both experimental and numerical methods are in excellent agreement with the theory.

Modelling of the rotors

The finite element method is very much used for the calculation of the complex structures is also efficient in dynamics of the rotors (Lalanne, 1998).

The elements of a rotor are: Disc, shaft and bearing. The kinetic energy T, the strain energy U and virtual work δW of external forces are calculated for all system elements to obtain the general equations of motion of a rotor.

It is necessary to define the finite elements making it possible modelling the rotors: discs, shaft, bearing and to represent external forces in particular those due to the unbalances.

The disc

The disk is assumed to be rigid. Only its kinetic energy is considered. The coordinate system x, y and z is connected to the coordinate system X, Y and Z through the angles ψ, θ and ϕ.

The angular velocity vector reflecting the position of the disc is written as:

$$\vec{\omega}^{R}_{R/R_0} = \begin{bmatrix} \omega_x \\ \omega_y \\ \omega_z \end{bmatrix} = \begin{bmatrix} -\dot{\psi}\cos\psi\sin\theta + \dot{\psi}\cos\theta \\ \dot{\theta} + \dot{\phi}\sin\psi \\ -\dot{\theta}_z\cos\theta_x\cos\theta_y + \dot{\theta}_x\sin\theta_y \end{bmatrix}_R \quad (1)$$

ω_x, ω_y and ω_z are the components of the angular velocity vector according to x, y and z . considering u and w coordinates of the center O of the disc along OX, OZ; the following coordinated OY remaining constant.

The disk mass is m_d

The inertia tensor is noted:

$$\mathrm{I}_{/o} = \begin{bmatrix} \mathrm{I}_{dx} & 0 & 0 \\ 0 & \mathrm{I}_{dy} & 0 \\ 0 & 0 & \mathrm{I}_{dz} \end{bmatrix}_{\mathrm{R}} \quad (2)$$

I_{dx}, I_{dy} and I_{dz} are the moments of inertia along the axis x, y and z respectively.

The general expression of the kinetic energy of the disc T_d is then written:

$$T_d = \frac{1}{2}m_d(\dot{u}^2 + \dot{w}^2) + \frac{1}{2}(I_{dx}\omega_x^2 + I_{dy}\omega_y^2 + I_{dz}\omega_z^2) \quad (3)$$

Or this expression can be simplified when the disc is symmetrical $I_{dx} = I_{dz}$. And when the angles θ and ψ are small and the angular velocity is constant, the Equation (3) becomes:

$$T_d = \frac{1}{2}m_d(\dot{u}^2 + \dot{w}^2) + \frac{1}{2}I_{dx}(\dot{\psi}^2 + \dot{\theta}^2) + \frac{1}{2}I_{dy}(\Omega^2 + 2\Omega\dot{\psi}\theta) \quad (4)$$

The term $\frac{1}{2}I_{dy}\Omega^2$, which is constant, has no influence on the equations of motion and represents the kinetic energy of the rotating disc at the rotational speed Ω, if all other displacement are zero. The last term $I_{dy}\Omega\dot{\psi}\theta$ is the gyroscopic effect (Coriolis).

The shaft

The shaft is assimilated to a beam of circular section and characterized by its kinetic and potential energies.

The expression of the kinetic energy is:

$$T_S = \frac{\rho S}{2}\int_0^L\left[\left(\frac{\partial u}{\partial t}\right)^2 + \left(\frac{\partial w}{\partial t}\right)^2\right]dy + \frac{\rho I}{2}\int_0^L\left[\left(\frac{\partial \psi}{\partial t}\right)^2 + \left(\frac{\partial \theta}{\partial t}\right)^2\right]dy + \rho I L\Omega^2 + 2\rho I\Omega\int_0^L\dot{\psi}\theta\,dy \quad (5)$$

ρ is the density, and S is the shaft section, I is the moment of inertia transverse (diametric).

The first integral of Equation 5 corresponds to the expression of the kinetic energy of a beam in bending, the second to the inertia effect due to the rotation and the last integral represents the gyroscopic effect.

The strain energy depends only on the stress and therefore the strain of the shaft relative to the support. In this calculation, one neglects the shear effects.

E is the Young modulus of the material, ε and σ represent respectively the strain and the stress, u^* and w^* are the displacements of the geometric center along the axes x and z (in the moving coordinate system).

The strain in bending of a point of the shaft with coordinate x and z in the reference frame R is

$$\varepsilon = \varepsilon_l + \varepsilon_{nl}$$

With the linear strain is given by:

$$\varepsilon_l = -x\frac{\partial^2 u^*}{\partial y^2} - z\frac{\partial^2 w^*}{\partial y^2} \tag{6}$$

The non linear strain is given by:

$$\varepsilon_{nl} = \frac{1}{2}\left(\frac{\partial u^*}{\partial y}\right)^2 + \frac{1}{2}\left(\frac{\partial w^*}{\partial y}\right)^2 \tag{7}$$

The general expression for the strain energy of the rotor in bending is then:

$$U = \frac{1}{2}\int_V \{\varepsilon\}^t [\sigma]\, d\tau \tag{8}$$

Where τ is the volume of the shaft and σ is the stress in bending.

The relationship between the stress and the strain is $\sigma = E\varepsilon$, are:

$$U = \frac{E}{2}\int_V \left(\varepsilon_1{}^2 + 2\varepsilon_l\varepsilon_{nl} + \varepsilon_{nl}{}^2\right) d\tau \tag{9}$$

Because of the symmetry of the shaft relative to the axes x and y, are obtained:

$$\int_V \varepsilon_{nl}\,\varepsilon_l\, d\tau = 0 \tag{10}$$

The third term of the integral (9) represents the effect of an axial force and is not considered in this study. Using the Equation 6 gives:

$$U = \frac{E}{2}\int_0^L \int_S \left(-x\frac{\partial^2 u^*}{\partial y^2} - z\frac{\partial^2 w^*}{\partial y^2}\right)^2 dS\, dy \tag{11}$$

$$U = \frac{E}{2}\int_0^L \int_S \left(x^2\left(\frac{\partial^2 u^*}{\partial y^2}\right)^2 + z^2\left(\frac{\partial^2 w^*}{\partial y^2}\right)^2 + 2xy\frac{\partial^2 u^*}{\partial y^2}\frac{\partial^2 w^*}{\partial y^2}\right) dS\, dy \tag{12}$$

By symmetry, the third term of Equation 12 is zero and, introducing the inertia of section:

$$\begin{aligned} I_x &= \int_S z^2\, dS \\ I_z &= \int_S x^2\, dS \\ \int_S xz\, dS &= 0 \end{aligned} \tag{13}$$

We find

$$U = \frac{E}{2}\int_0^L \left(I_z\left(\frac{\partial^2 u^*}{\partial y^2}\right)^2 + I_x\left(\frac{\partial^2 w^*}{\partial y^2}\right)^2\right) dy \tag{14}$$

To avoid periodic terms, explicit function of time, it is necessary given considering the properties of bearings, to express the strain energy depending on u and w components of the displacement in the initial frame.

The passage of u^*, w^* at u, w is:

$$\begin{cases} u^* = u\cos\Omega t - w\sin\Omega t \\ w^* = u\sin\Omega t + w\cos\Omega t \end{cases} \tag{15}$$

Replacing u * and w * by their values (15):

$$U = \frac{E}{2}\int_0^L \left(I_z\left(\cos\Omega t\frac{\partial^2 u}{\partial y^2} - \sin\Omega t\frac{\partial^2 w}{\partial y^2}\right)^2 + I_x\left(\sin\Omega t\frac{\partial^2 u}{\partial y^2} + \cos\Omega t\frac{\partial^2 w}{\partial y^2}\right)^2\right) dy \tag{16}$$

$$U = \frac{E}{2}\int_0^L I_z\left(\cos^2\Omega t\left(\frac{\partial^2 u}{\partial y^2}\right)^2 + \sin^2\Omega t\left(\frac{\partial^2 w}{\partial y^2}\right)^2 - 2\frac{\partial^2 u}{\partial y^2}\frac{\partial^2 w}{\partial y^2}\cos\Omega t\sin\Omega t\right) + I_x\left(\sin^2\Omega t\left(\frac{\partial^2 u}{\partial y^2}\right)^2 + \cos^2\Omega t\left(\frac{\partial^2 w}{\partial y^2}\right)^2 + 2\frac{\partial^2 u}{\partial y^2}\frac{\partial^2 w}{\partial y^2}\cos\Omega t\sin\Omega t\right) \tag{17}$$

For a symmetrical shaft, the expression of the strain energy becomes:

$$U = \frac{E}{2}\int_0^L I_z\left((\cos^2\Omega t + \sin^2\Omega t)\left(\frac{\partial^2 u}{\partial y^2}\right)^2 + (\sin^2\Omega t + \cos^2\Omega t)\left(\frac{\partial^2 w}{\partial y^2}\right)^2\right) dy \tag{18}$$

Finally:

$$U = \frac{E}{2}\int_0^L I_z\left(\left(\frac{\partial^2 u}{\partial y^2}\right)^2 + \left(\frac{\partial^2 w}{\partial y^2}\right)^2\right) dy \tag{19}$$

Bearings

A bearing has the characteristics of stiffness and damping in the two planes. The forces applied by the bearings are due to displacement of the shaft relative to

the support.

The virtual work δW_P of external forces acting on the shaft of the first bearing is written as:

$$\begin{aligned}\delta W_P = &-k_{xx}u\delta u - k_{xz}w\delta u - k_{zz}w\delta w - k_{zx}u\delta w \\ &- c_{xx}\dot{u}\delta u - c_{xz}\dot{w}\delta u - c_{zz}\dot{w}\delta w - c_{zx}\dot{u}\delta w\end{aligned} \quad (20)$$

Similarly to the second bearing

Mass unbalance

The initial unbalance is generally distributed so as continuous on the rotor. The expression of the kinetic energy T_b of the unbalance is:

$$T_b = \frac{m_b}{2}(\dot{u}^2 + \dot{w}^2 + \Omega^2 d^2 + 2\Omega\dot{u}\, d\cos\Omega t - 2\Omega\dot{w}\, d\sin\Omega t) \quad (21)$$

m_b Is the unbalance mass.

The term $\Omega^2 d^2/2$ is constant and will not intervene in the equations. The mass of the unbalance is negligible compared to the rotor mass; the expression of the kinetic energy can be approximated by:

$$T_b \approx m_b\,\Omega d(\dot{u}\cos\Omega t - \dot{w}\sin\Omega t) \quad (22)$$

The terms of the kinetic energy, strain energy and virtual work being established. The expressions of displacements in the X and Z directions are respectively set in the (separation of variables method):

$$\begin{aligned}u(y,t) &= f(y)q_1(t) = f(y)q_1 \\ w(y,t) &= f(y)q_2(t) = f(y)q_2\end{aligned} \quad (23)$$

Where q_1 and q_2 are generalized independent coordinates.

The second order derivative of *u* and *w* displacements is necessary to express the elastic energy of the shaft:

$$\begin{aligned}\frac{\partial^2 u}{\partial y^2} &= \frac{d^2 f(y)}{dy^2}q_1 = h(y)q_1 \\ \frac{\partial^2 w}{\partial y^2} &= \frac{d^2 f(y)}{dy^2}q_2 = h(y)q_2\end{aligned} \quad (24)$$

The functions $g(y)$ and $h(y)$ represents the first derivative and the second derivative respectively. Given that the angular displacements, ψ and θ are small, they are approached by:

$$\begin{cases}\theta = \dfrac{\partial w}{\partial y} = \dfrac{df(y)}{dy}q_2 = g(y)q_2 \\ \psi = -\dfrac{\partial u}{\partial y} = -\dfrac{df(y)}{dy}q_1 = -g(y)q_1\end{cases} \quad (25)$$

The displacement function f is chosen to represent exactly the form of the first mode of a constant section beam in bending on two simply supported situated at its ends.

$$f(y) = \sin\frac{\pi y}{L} \quad (26)$$

Hence,

$$g(y) = \frac{\pi}{L}\cos\frac{\pi y}{L} \quad (27)$$

$$h(y) = -\left(\frac{\pi}{L}\right)^2 \sin\frac{\pi y}{L} \quad (28)$$

Substituting in the expressions of (25) where (4), we find: The kinetic energy of the disk T_D can be written as follows:

$$\begin{aligned}T_D = \frac{1}{2}\left[M_D f^2(y_{disk}) + I_{Dx} g^2(y_{dick})\right]\left(\dot{q}_1^2 + \dot{q}_2^2\right) \\ - I_{Dy}\Omega\, g^2(y_{dick})\,\dot{q}_1\dot{q}_2\end{aligned} \quad (29)$$

The expression for the kinetic energy of the shaft *Ts* is:

$$\begin{aligned}T_S = \frac{1}{2}\left[\rho S\int_0^L f^2(y)\,dy + \rho I\int_0^L g^2(y)\,dy\right]\left(\dot{q}_1^2 + \dot{q}_2^2\right) \\ - 2\rho I\Omega\int_0^L g^2(y)\,dy\,\dot{q}_1 q_2\end{aligned} \quad (30)$$

The strain energy of the shaft is:

$$U_S = \frac{EI}{2}\int_0^L h^2(y)\,dy\left(q_1^2 + q_2^2\right) \quad (31)$$

The kinetic energy of the ensemble disk - rotor is given by:

$$\begin{aligned}T_{DS} = T_S + T_D = &\left[\frac{1}{2}\left(M_D f^2(y_{disk}) + I_{Dx} g^2(y_{dick})\right)\right. \\ &\left. + \frac{1}{2}\left(\rho S\int_0^L f^2(y)\,dy + \rho I\int_0^L g^2(y)\,dy\right)\right]\left(\dot{q}_1^2 + \dot{q}_2^2\right) \\ &- I_{Dy}\, g^2(y_{dick}) + 2\rho I\int_0^L g^2(y)\,dy\;\Omega\dot{q}_1\, q_2\end{aligned} \quad (32)$$

The kinetic energy of the unbalance is:

$$T_u = m_b\, d\Omega\, f(y_{bal})(\dot{q}_1\cos\Omega t - \dot{q}_2\sin\Omega t) \quad (33)$$

Where T_d, T_a, T_b are the respective kinetic energies of the

disc, shaft, of the unbalance.

The application of Lagrange equations:

$$\frac{d}{dt}\left(\frac{\partial T_c}{\partial \dot{q}_i}\right)-\frac{\partial T_c}{\partial q_i}+\frac{\partial U}{\partial q_i}=\delta W_i \quad (34)$$

avec i=1, 2.

Which in general form are written:

$$\left[M_D f^2(y_{disk})+I_{Dx} g^2(y_{dick})+\rho S\int_0^L f^2(y)\,dy+\rho I\int_0^L g^2(y)\,dy\right]\ddot{q}_1 - \left[I_{Dy}\, g^2(y_{dick})+2\rho I\int_0^L g^2(y)\,dy\right]\Omega\dot{q}_2+k\,q_1=m_b\,d\,\Omega^2\,f(l_1)\sin\Omega t \quad (35)$$

$$\left[M_D f^2(y_{disk})+I_{Dx} g^2(y_{dick})+\rho S\int_0^L f^2(y)\,dy+\rho I\int_0^L g^2(y)\,dy\right]\ddot{q}_2 + \left[I_{Dy}\, g^2(y_{dick})+2\rho I\int_0^L g^2(y)\,dy\right]\Omega\dot{q}_1+k\,q_2=m_b\,d\,\Omega^2\,f(l_1)\cos\Omega t$$

Solving this system of equations provides the expressions of frequencies and deflections of the tree line in each of its points.

Modal analysis and numerical simulation

It is about the calculation of the dynamic behaviour of a rotor step by step in time. The objective is to present a model of calculation using a simplified approach. The construction of the grid is made with ANSYS software starting from the characteristics of the various elements of the rotor. Modelling by finite elements requires the supply of data relating to the geometry (coordinated nodes), boundary conditions, and description of the elements (disc, bearing, and additional elements) of mechanical characteristics of materials and bearing, function of the rotation speed and on the information relative to the excitations.

The finite element Model of the rotor is carried out with the code ANSYS. The shaft is discredited by the beam element to 4 degrees of freedom by node: two displacements U and W and two rotations according to Y and Z. The disc is supposed to be rigid. This model makes it possible to carry out temporal simulations of the dynamic behaviour of the rotor.

The disc is assumed to be perfectly rigid and it's modeling using a pipe element (Pipe16). To model the shaft using the beam element (Beam189). For modeling the bearings are used spring-damper element (Combin14).

The finite element model of the rotor consists of a shaft, disc and bearings. The length and outer diameter of the shaft is $L=1.4\ m$ r = 0.15 m respectively. The inner diameter and outer diameter of the disc is r_1 = 0.15 m and r_2 = 0.625 m respectively.

The material is a special steel assumed homogeneous and isotropic, with density $\rho_d = 7850\ kg/m^3$, Poisson's ratio $\nu = 0.3$ and elastic Young's modulus $E_a = 248\ GPa$.

The disc is a special steel assumed to be homogeneous, isotropic and having $\rho_d = 7850\ kg/m^3$, Poisson's ratio $\nu = 0.3$ and elastic Young's modulus $E_a = 248\ GPa$.

The stiffness and the damping for the first bearing is:

$$k_{yy}=1.10^8\ N/m,\quad k_{zz}=8.10^7\ N/m,$$
$$c_{yy}=1{,}2.10^4\ N.s/m,\quad c_{zz}=8.10^3\ N.s/m$$

The stiffness and the damping for the second bearing is:

$$k_{yy}=7.10^8\ N/m,\quad k_{zz}=5.10^7\ N/m,$$
$$c_{yy}=8.10^3\ N.s/m,\quad c_{zz}=6.10^3\ N.s/m$$

The calculation is made from the discretization of the shaft into several elements, once the data is entered the geometric model is established and it resulted in the rotor mesh (Figure 1). All numerical data on the mesh of the rotor is summarized in Table 1. The model comprises 51 nodes, or 204° of freedom and ale modal base consists of five modes.

Boundary conditions

The characterization of the rotor can be made by its decomposition into flexible finite element and therefore study node by node boundary conditions.

During the movement, the center line of the shaft does not remain confused with the original right are (Ux, Uy, Uz) displacements of the shaft, Uy and Uz are variables while Ux is considered as constant since only the shaft deflection movements are studied.

So for the nodes of the two bearings we annul all degrees of freedom, for the nodes of the rotor we annul the degrees of freedom of translation and rotation along the x axis (Figure 2), there are only four degrees of freedom per node, two rotations according y and z, and two translations according y and z.

Evolution of the stress

A force is applied on the disc, and thereafter determines the equivalent Von Mises stress in static analysis (Figure 3). The concentration of stress is observed at the connection between the shaft and the disc. The maximal stress is 201 Mpa; this is a sensitive area for the appearance of defects.

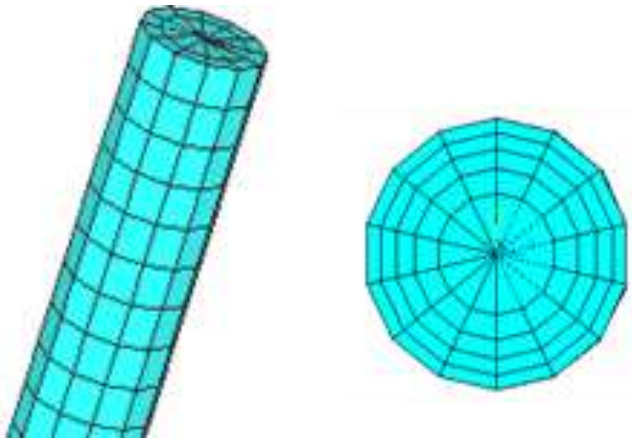

Figure 1. Rotor meshing.

Table 1. the number of element, nodes and degrees of freedom of the rotor.

Structure	Element	Nodes	Degrees of freedom
Rotor	30	51	204

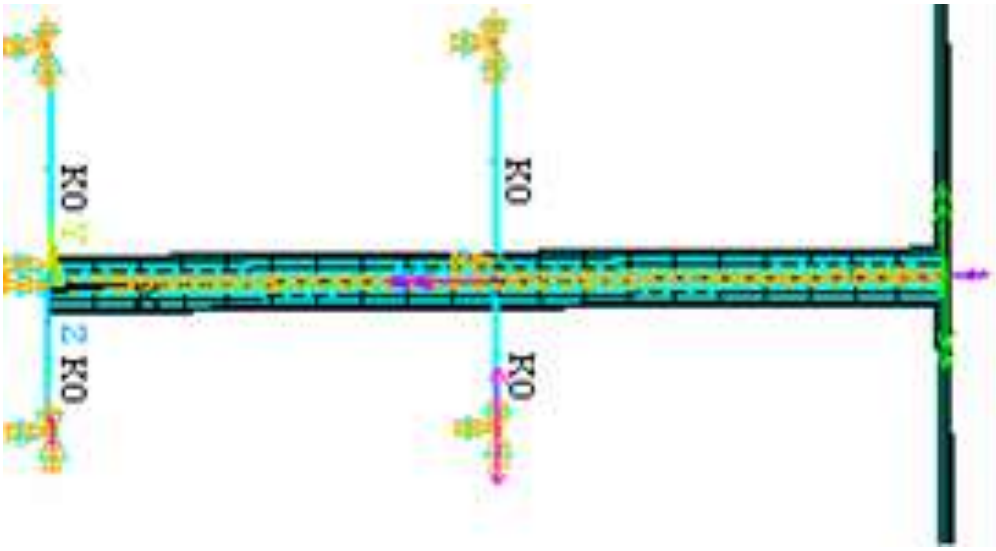

Figure 2. Boundary conditions of the rotor.

Modal analysis

The modal base consists of five modes. The objective of this study is to determine the eigen frequencies and eigen modes and the stresses of bending vibration of the rotor. The eigen frequencies are represented on the Table 2.

The modal base contains five modes. The allure of the three modes of the rotor and their orbits of mode shapes at any rotational speed is shown in Figures 4 to 6. These modes are characterized by local bending.

Campbell diagram

The critical speeds are given by the intersection points of the excitation sources (Harmonics 1, 4, 5 ...) with the natural modes to direct precession and reverse precession.

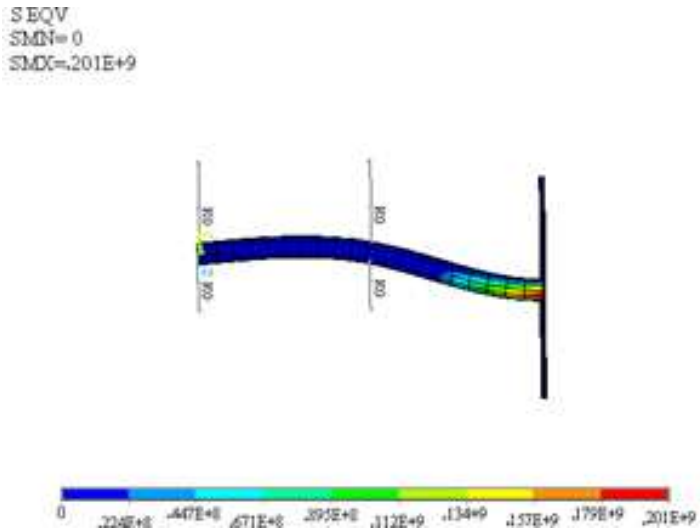

Figure 3. Evolution of the Von Mises equivalent stress.

Table 2. Eigen frequencies of the rotor.

Mode	1	2	3	4	5
Frequency (Hz)	27	42	120	220	310

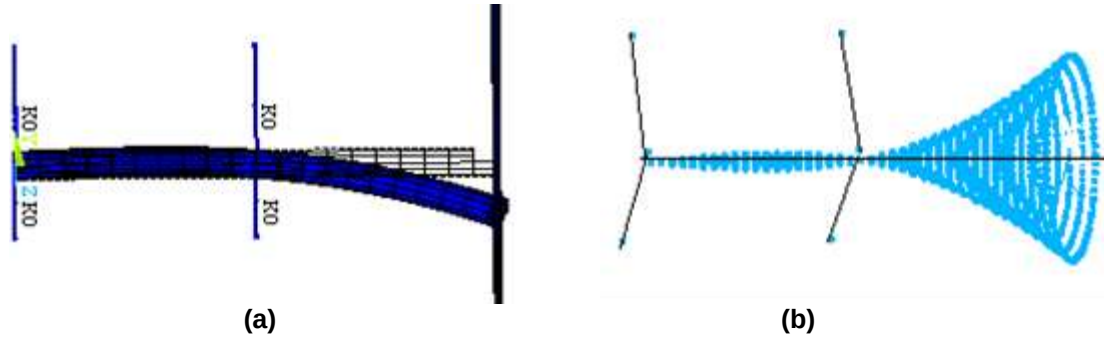

(a) **(b)**

Figure 4. The first mode (a) The first mode shapes (f=27Hz, Dmax =0.0051); (b) The orbits of mode shapes at 258 rpm.

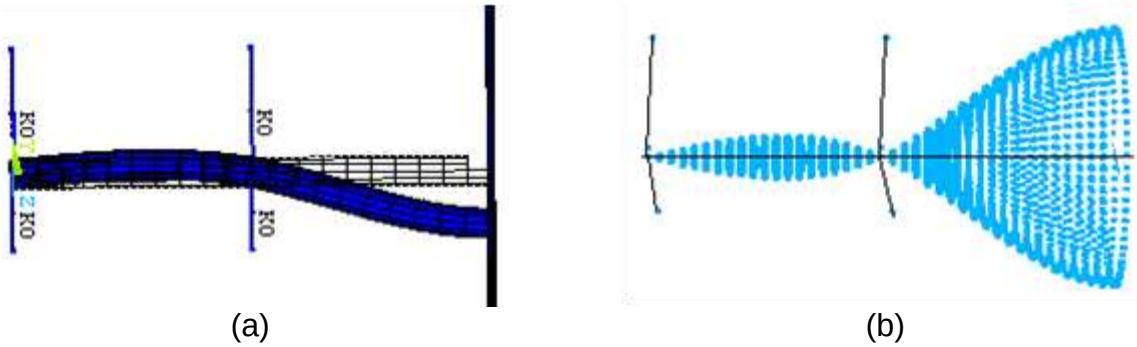

(a) (b)

Figure 5. The third mode (a) The third mode shapes (f = 120 Hz, Dmax = 0.0062); (b) The orbits of mode shapes at 1146.5 rpm.

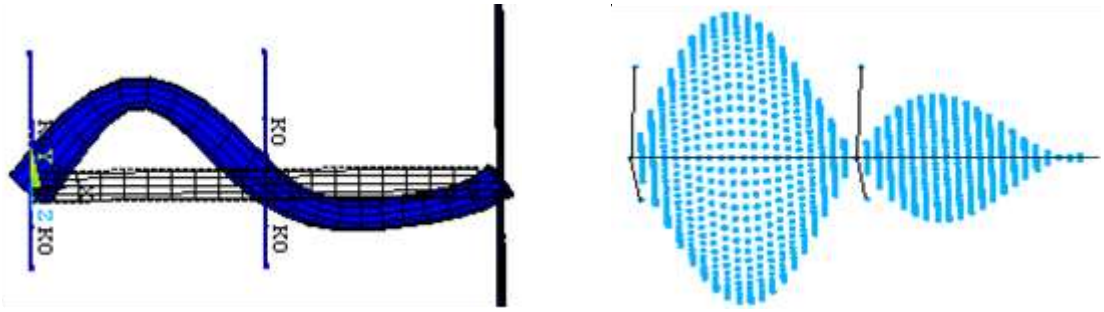

(a) (b)

Figure 6. The five mode (a) The five mode shapes (f = 310 Hz, Dmax = 0.042); (b) The orbits of mode shapes at 2262 rpm.

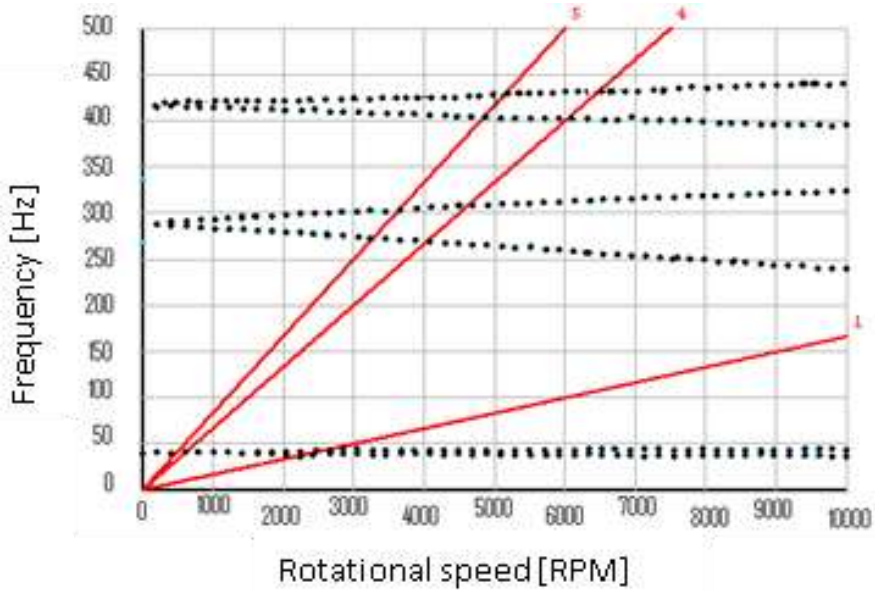

Figure 7. The diagram of Campbell.

We get Campbell diagram (Lalanne, 1998; Genta, 1992; Muszynska, 1996; Mogenier, 2012; Saad and Seamus, 2011).

The diagram of Campbell (Figure 7) shows that the first critical speeds (for the harmonic in the order 1, 4 and 5). For the harmonic of order 1, which corresponds to the first mode of the shaft at the speed of 2500 rev/min (40 Hz)? For the harmonic of order 4, the first critical speed is 600 rev/min (40 Hz); the second critical speed is 4000 rev/min (270Hz) and finally 4500 rev/min (310 Hz).

Spectrum of frequency response

The results in the Fourier spectrum Figure 8 are obtained from the numerical simulation. The rotor is subject to an unbalance of 0001 kg and an asynchronous force with the intensity is 1 N placed at node number 19 for L = 1.4 m, for a rotational speed equal to 500 rpm. After running, the responses of each node is obtained, the results of the responses at the node Number 19 are presented as graphs showing the spectral response.

Figure 8 represents the frequency response curve for speeds of rotation from 0 to 500 RPM .The frequency at which the peak response occurs 18 and 37 Hz is. The first frequency is explained by an initial shock due to the applied force. The second frequency corresponds to the frequency of the critical speed of the associated linear system, it amounts to the initial unbalance.

MATERIALS AND METHODS

Vibration monitoring generally used to monitor in real time and without interruption the vibration behavior of rotating machines. A

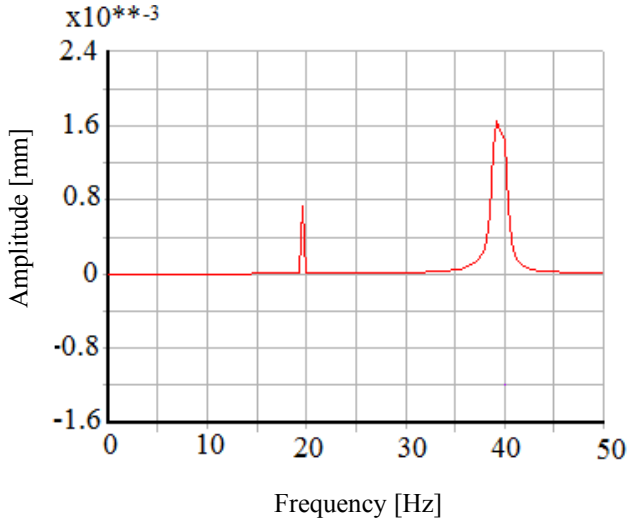

Figure 8. Spectrum of frequency response.

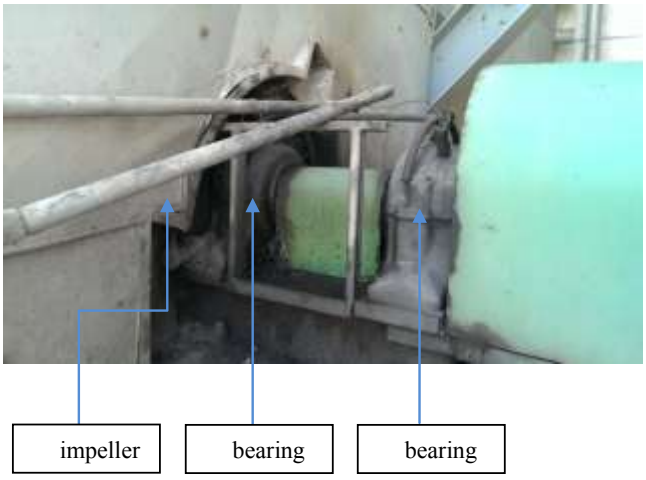

Figure 9. The combustion air ventilator components.

wide variety of techniques have been used for fault detection and diagnosis in rotating machinery. These techniques can be classified into frequency domain, time domain, time-frequency domain and other and techniques (Kumar et al., 2013; Kumar and Kumar, 2014; Jalan and Mohanty, 2009; Yang and Court, 2009, Chellil et al., 2015). This study will primarily investigate techniques based on the time domain, frequency domain and time-frequency domain [Ding et al., 2016] detailed spectral analysis is presented by Yamamoto et al. (2016), the results clearly show the feasibility of this experimental intelligent diagnostic approach for measuring vibration and unbalance fault detection in rotating machinery.

A case of industrial survey was treated for validate the approach and to show that in some cases exceeding the thresholds imposed by the standards represent a defect synonymous. We will make the establishment of the rotor vibration analysis following the method of OFF LINE system. The measurements are performed at regular time intervals (periodically) by portable systems increasingly informatics. The aim of this work is to do a vibration analysis (monitoring and diagnostic) to study vibration phenomena emerged the rotor.

The combustion air ventilators have the task of feeding the steam generator combustion area required in power plants. They aspire outside air and do to the burners through air preheater. In this case the ventilator is composed of a shaft, impeller and two bearings (Figure 9). The high quality steel shaft, the impeller is high quality steel; it is mounted on a cylindrical seat on the shaft by means of an interference fit oil seal. The shaft is mounted in two bearings at bearings type FAG SN 328 and FAG 22328 ES.

Equipments used for test

The measurements were realized using the following equipment.

Vibration sensor

This is an AS-065 piezoelectric accelerometer connected to the VIBROTEST 60 analyzer manifold. This sensor is used to measure vibration acceleration (Figure 10b).

Vibrotest 60 analyzer

The VIBROTEST 60 (Figure 10c) is a practical acquisition apparatus for making: global vibration measurements, process parameter, time signals and spectral signals.

The implementation of the accelerometer on the machines is very important. Each measurement companion must be performed at specific points and always the same. We try to close as possible points of measurements of bearings; it allowed us to get the most loyal mechanical defects images.

RESULTS AND DISCUSSION

Figure 11a and b represent the measurements of vibrations in the horizontal direction (Bearing 1) and the vertical direction (Bearing 2) of the pump.

The first spectral line in the first spectrum (Figure 4a) has an amplitude of 0.47 mm/s, this value exceeds the warning threshold, the frequency of this line is 9.88 Hz (95 rev / min), the speed is the rotational speed of the rotor.

The 2nd spectral line in the same spectrum (Figure 4a) has amplitude of 0.9 mm/s and a frequency 153.76 Hz. This value is below the alert threshold and not a danger.

The first spectral line in the first spectrum (Figure 4b) has an amplitude of 0.235 mm/s when it exceeds the threshold. The frequency of this line is 50 Hz (477.70 rev / min), the speed is the speed of rotation of the rotor.

The 2nd spectral line in the same spectrum (Figure 4b) has an amplitude of 0.14 mm/s and a frequency 153.76 Hz. This value is below the alert value and is not dangerous.

The 1st two spectral lines on the two spectra (Figure 4a and b) are on the same frequency of rotation of the shaft and we have high vibration speed on the three directions of measurements, so this symptom tells us about the existence of a defect unbalance.

The two spectral lines that follow have frequencies equal to twice the rotation frequency of the shaft, the

(a)

(b)

(c)

Figure 10. Equipments used for test (a) Equipments used for test measurement of vibration; (b) Accelerometer AS-065; (c) Vibrotest 60.

♦ Signal of Bearing 1 (Horizontal directio

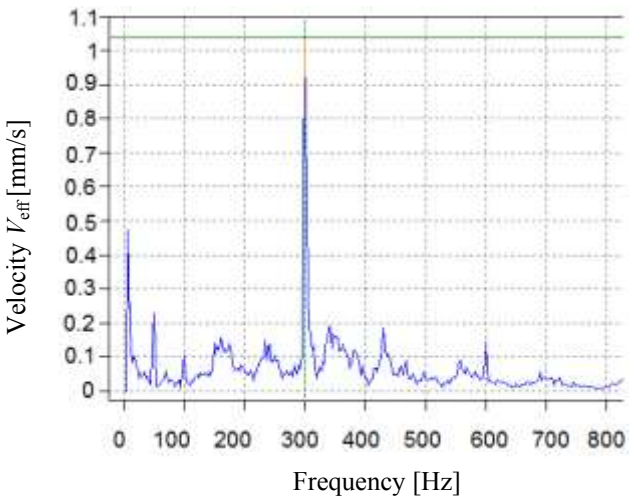

(a)

♦ Signal of Bearing 2(Vertical direction)

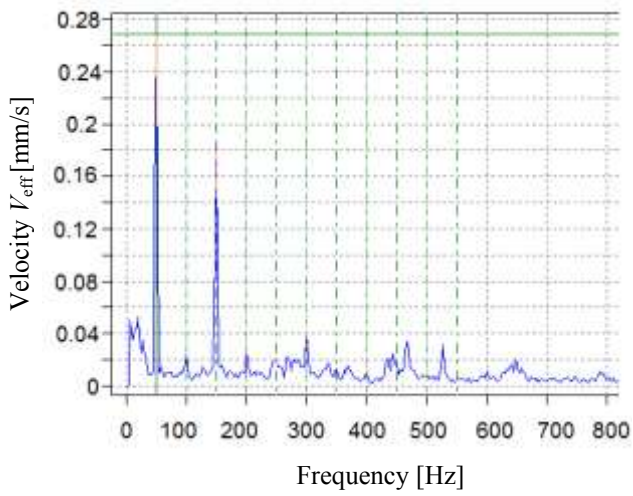

(b)

Figure 11. Spectral responses of the bearings (a) Horizontal bearing1 spectrum; (b) Vertical bearing 2 spectrums.

amplitude of the vibration levels are below the warning threshold, they are due to the significance of this imbalance in the two bearings of the pump shaft. Once the fault is repaired the vibration must disappear.

Conclusion

The model of finite elements of the rotor was designed starting from a well defined geometry. An effective interpretation of the frequencies and modal deformations

of the model were simulated. The distribution of the stress along the rotor was identified. In the present case, the maximum stress is 201 Mpa were concentrated at the connection between the shaft and the disc. The differences on the level of the maximum amplitude of the vibrations can be easily reduced significantly with the geometrical model. Nevertheless, as the critical speed depends on the considered shape, one can determine the intensity of the amplitude on the response curve to unbalance. The layout of the response to an unbalance presents brutal increases in the amplitude of vibration of the rotor. In this article, an detection system based on industrial signals treated in the frequency domain is proposed. The results were presented to identify and detect unbalanced faults in bearing. The analysis of measurement results shows the presence of an unbalance fault on the rotating machinery. This defect is the cause of a long shutdown and poor conditions present during shutdown, it is recommended to remedy a bearing balancing the rotating machinery.

Conflict of Interests

The authors have not declared any conflict of interests.

REFERENCES

Al Majid A, Allezy A, Dufour R (2003). Metric of MDOF systems in high transient motion, Proceedings of ASIVIE Design Engineering Technical Conferences, 2-6 September. Chicago. USA. P 6.

Chellil A (2015). Condition Monitoring for Controlling the Stability of the Rotating Machinery. Int. J. Mech. Aerosp. Ind. Mech. Man. Eng. 9(12):2030-2035.

Ding Y, He W, Chen B, Zi Y, Selesnick IW (2016). Detection of faults in rotating machinery using periodic time-frequency sparsity. J. Sound Vib. 382:357-378.

Duchemin M (2003). Contribution à l'étude du comportement dynamique d'un rotor embarqué. Thèse de doctorat de l'INSA-Lyon.

Genta G (1992). A fast modal technique for the computation of the Campbell diagram of multi-degree-of-freedom rotors". J. Sound Vib. 155(3):385-402.

Jalan AK, Mohanty AR (2009). Model based fault diagnosis of a rotor bearing system for misalignment and unbalance under steady state condition. J. Sound Vib. 327:604-622.

Kumar PS, Abraham A, Bensingh RJ, Ilangovan S (2013). Computational and Experimental analysis of a Counter-Rotating Wind Turbine system. J. Sci. Ind. Res. 72(05):300-306.

Kumar SS, Kumar MS (2014). Condition Monitoring of rotating machinery through Vibration Analysis. J. Sci. Ind. Res. 73(04):258-261.

Lalanne M, Ferraris G (1998). Rotordynamics prediction in engineering. 2nd Edition. Chichester, John Wiley. P 254.

Mogenier G, Baranger T, Ferraris G, Dufour R, Durantay L (2012). The problem of complex shape tracking in a Campbell Diagram or how to overcome crossing/veering phenomena. 10th International Conference on Vibrations in Rotating Machinery. pp. 257-267.

Muszynska A (1996). Forward and backward precession of a vertical anisotropically supported rotor. J. Sound Vib. 192(1):207-222.

Nelson HD (1980). A Finite Rotating Shaft Element Using Timeshenko Beam Theory. J. Mech. Des. Trans. ASME 102:793-803.

Saad SA, Seamus DG (2011). Modal correlation approaches for general second-order systems: Matching mode pairs and an application to Campbell diagrams. J. Sound Vib. 330(23):5615-5627.

Si-Chaib M, Chellil A, Nour A, Saci R, Chikh N, Chevalier Y (2008). Numerical and experimental investigation of the dynamic behavior a vertical rotor. 15th International Congress on Sound and Vibration. Daejeon. Korea. Proceed. ICSV 15:2347-2354.

Stodola A (1927). Steam and Gas Turbines. McGraw-Hill. New York. Vol. I.

Tran DM (1981). Etude du comportement dynamique des rotors flexibles. Thèse Université C. Bernard. Lyon.

Vance JM, Murphy BT, Tripp HA (1987). Critical speeds of turbo machinery; computer predictions versus experimental measurements. J. Vib. Acoust. 109:1-7.

Wei L, Zhencai Z, Fan J, Gongbo Z, Guoan C (2015). Fault diagnosis of rotating machinery with a novel statistical feature extraction and evaluation method. Mech. Syst. Signal Process. 50(51):414-426.

Yamamoto GK, da Costa C, da Silva Sousa JS (2016). A smart experimental setup for vibration measurement and imbalance fault detection in rotating machinery. Case Stud. Mech. Syst. Signal Process. 4:8-18.

Yang W, Court R (2013). Experimental study on the optimum time for conducting bearing maintenance. Measurement 46:2781-2791.